

Empirical estimates of CCN from aerosol optical properties at four remote sites

A. Jefferson

Cooperative Institute for Research in Environmental Science (CIRES), University of Colorado, Boulder, CO, USA
NOAA Earth System Research Laboratory, Boulder, CO, USA

Received: 12 March 2010 – Published in Atmos. Chem. Phys. Discuss.: 8 April 2010

Revised: 14 June 2010 – Accepted: 6 July 2010 – Published: 23 July 2010

Abstract. This study presents an empirical method to estimate the CCN concentration as a function of percent supersaturation. The aerosol optical properties, backscatter fraction and single scatter albedo, function as proxies for the aerosol size and composition in a power law relationship to CCN. This method is tested at four sites with aged aerosol: SGP (Oklahoma, USA), FKB (Black Forest, Germany), HFE (Hefei, China) and GRW (Graciosa, Azores). Each site represents a different aerosol type and thus demonstrates the method robustness and limitations. Good agreement was found between the calculated and measured CCN with slopes between 0.81 and 1.03 and correlation coefficients (r^2 values) between 0.59 and 0.67. The fit quality declined at low CCN concentrations.

1 Introduction

The highest uncertainty in estimates of climate forcing is the indirect forcing associated with clouds (Solomon et al., 2007). Clouds present a formidable challenge to parameterize their spatial variance, lifetime, albedo, precipitation and formation. The full characterization of aerosol activation into cloud droplets as a function of the percent supersaturation is one such challenge. Calculation of aerosol activation to cloud condensation nuclei concentration (CCN) using Köhler's equation requires knowledge of the size-dependent aerosol composition. Because of the resource and computationally – intensive nature of these measurements and models, long term monitoring of aerosol size-dependent composition for different aerosol types and regions is not currently

feasible. A widely used simplification of the Köhler equation is the κ -Köhler model developed by Petter and Kriedenweis (2007), which uses a single parameter, κ , to relate the aerosol water activity and solute concentration. Several studies build upon this model by using proxies for κ such as the aerosol hygroscopic growth (Gasparini et al., 2006b; Good et al., 2009; Ervens et al., 2007; Petters et al., 2009), soluble fraction and mixing state (Ervens et al., 2009), fraction of refractory material or organic composition (Shinozuka et al., 2009). Other empirical methods relate the CCN to the aerosol extinction or AOD (Gahn et al., 2004, 2006; Andreae, 2008).

This study presents an empirical model of the CCN concentration from the aerosol optical properties. The model is a power law fit of the CCN data that uses the aerosol backscatter fraction and the single scatter albedo as proxies for the aerosol size and composition. The model fits empirical estimates of CCN for four regional sites from the US Department of Energy Atmospheric Radiation Measurement Climate Research Facilities (ACRF). Each of these sites represents a different aerosol type and shows both the robustness and limitations of this method in estimating CCN. The sites in this study are the Southern Great Plains, Oklahoma (SGP), the Murg Valley, Germany (FKB), Shouxian, China (HFE), and Graciosa Island, Azores (GRW). Because a broad network of aerosol optical measurements already exists, this empirical method has the potential to provide data for model assimilation and validation of CCN processes on local to global scales. The parameters derived from this empirical method can contribute to a regional climatology of CCN properties. While not a substitute for direct measurements of CCN, this method can be utilized as a proxy for CCN where measurements do not exist.



Correspondence to: A. Jefferson
(anne.jefferson@noaa.gov)

Table 1. Field site locations, dates of operation, range of % super saturation, average (± 1 std dev.) of aerosol sub μm scattering coefficient (σ_{sp}), backscatter fraction and single scatter albedo at 450 nm.

Site	lon, lat	Date	% SS range	σ_{sp}	BSF	SSA
Oklahoma, SGP	36°36' N, 97°29' W	10 Feb–20 May 2009	0.19–0.82	47 (51)	0.12 (0.02)	0.92 (0.04)
Black Forest, FKB	48°32' N, 08°23' E	31 May–6 Dec 2007	0.26–0.83	51 (38)	0.12 (0.02)	0.88 (0.04)
Hefei, HFE	32°33' N, 116°46' E	26 Jul–23 Aug 2008	0.40–0.88	118 (68)	0.10 (0.01)	0.89 (0.03)
Graciosa, GRW	39°5' N, 28°1' W	20 Apr–27 Sep 2009	0.21–0.86	11 (8)	0.09 (0.02)	0.88 (0.06)

2 Measurements

In-situ measurements of aerosol optical properties and CCN were conducted at the four ARM Climate Research Facility (ACRF) sites. The site location and measurement duration period are listed in Table 1 as well as the aerosol scattering coefficient, backscatter fraction and single scattering albedo of each site over the measurement period. SGP is a permanent facility and the other three sites, FKB, GRW and HFE, are part of a mobile facility with varying operations periods. Data sets are limited by the deployment period and instrument operation. Detailed information about each site is located on the ACRF web site at <http://www.arm.gov/sites>. SGP is located in an agricultural region in the central US. FKB is located in the Black Forest of Germany in a valley with agriculture and surrounded by hills with coniferous forests. HFE is in the Anhui Province of China with mixed agricultural, pollution and dust aerosol sources. GRW is a remote marine site in the Atlantic Ocean with periodic local pollution from airport traffic and long-range transport from Europe.

The measurement configuration was similar at each site. Sheridan et al. (2001) gives a detailed description of the aerosol optical measurements at SGP. Sample air enters the system at ~ 800 lpm via a 10 m stack. The sample air splits between the five, 30 lpm sample lines. The sample for the optical measurements flows through an impactor which size segregates the aerosol between sub μm and sub 10 μm aerosol in 30 min intervals. A pickoff from one of the 30 lpm sample lines diverts a 500 ccm flow to the CCN.

The properties of the aerosol total scattering (7–170°) and backscattering (90–170°) coefficients at 450, 550 and 700 nm radiation are measured with a TSI model 3563 integrating nephelometer. The aerosol light absorption coefficient was measured using a filter-based Radiance Research PSAP at 470, 528 and 660 nm radiation. Corrections based on light truncation in the nephelometer and aerosol scatter from the PSAP filter were performed (Anderson and Ogren, 1998 and Bond et al., 1999). The 470 nm absorption coefficient was wavelength adjusted to 450 nm so that it would coincide with the scattering coefficient wavelength of the nephelometer. Discussion of uncertainty in the nephelometer total and backscatter coefficients can be found in Anderson et

al. (1996) and Heintzenberg et al. (2006). Studies of the uncertainty in the psap absorption coefficient can be found in Sheridan et al. (2005) and Virkkula et al. (2005).

The CCN at several supersaturations was measured using a DMT CCN counter (Roberts and Nenes, 2005). The percent supersaturation (% SS) of the instrument was stepped through 7 intervals every 30 min with 5 min at each setting in a pyramid form. The CCN instrument was serviced and calibrated at the beginning and end of each deployment for the mobile facility and bi-annually for the SGP site. The % SS in the CCN was calculated using a heat transfer and fluid dynamics model flow model (Lance et al., 2006). The model uses the calibrated temperature, pressure and flows in the instrument to calculate the % SS. Small variations in the % SS will arise from changes in the column thermal properties in the instrument. Rose et al. (2008) has an extensive discussion that compares model and salt calibration calculations of the instrument % SS and uncertainty associated with thermal properties.

3 Empirical method

The empirical fit uses a power law, as derived by Twomey (1959), to parameterize the CCN activity spectra.

$$\text{CCN} (\% \text{ SS}) = C (\% \text{ SS})^k \quad (1)$$

The fit used values of % SS in the range of 0.2 to 0.9, with variance of $\pm 0.1\%$ SS between sites. At higher % SS the k parameter decreases (Khvorostyanov and Curry, 2006) and below this range the uncertainty in the % SS increases (Rose et al., 2008). Fit parameters with poor goodness of fit chi-square values were rejected as they usually indicated noisy activation spectra or spikes in the data. The C and k fit parameters were then fit to linear correlations with the sub micron aerosol backscatter fraction and single scatter albedo at 450 nm as follows.

$$C/\sigma_{\text{sp}}(450 \text{ nm}) = m \cdot \text{BSF}(450\text{nm}) + b \quad (2)$$

$$k = p \cdot \text{SSA}(450 \text{ nm}) + d \quad (3)$$

Here, C is normalized to the submicron total angular scatter at 450 nm, σ_{sp} (450 nm), SSA (450 nm) is the aerosol sub

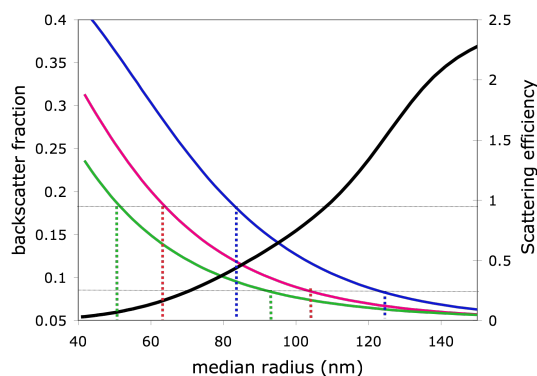


Fig. 1. Mie calculations of the aerosol scattering efficiency (black line) and backscatter fraction at three lognormal distribution widths of $s = 1.4$ (blue), 1.5 (red) and 1.6 (green). The dashed lines show the range of backscatter values used in this study.

μm single scattering albedo at 450 nm , m and p are the slopes and b and d are the offsets of the linear correlations. The empirical fit calculates CCN by replacing the C and k fit parameters with the linear fits in Eqs. (2) and (3). In these fits BSF ranged between 0.08 and 0.18 and SSA was limited to 0.8 to 1.0 . In order to screen for large accumulation mode dust particles that may skew the fits, data with scattering Ångström exponents below 1.0 were eliminated. Note that dust particles with Ångström exponents greater than 1.0 or diameters less than about $0.5\ \mu\text{m}$ were part of the analysis.

The suitability of using aerosol optical measurements to estimate CCN depends on the overlap between the critical aerosol size for activation to CCN and the aerosol scattering efficiency. The empirical fit maximizes this overlap by selecting sub μm aerosol at the shortest wavelength of the nephelometer, 450 nm . Mie scattering calculations of the aerosol backscatter fraction and scattering efficiency in Fig. 1 show the probable size range of the nephelometer measurements for different lognormal widths. Aerosol activation depends on both the Kelvin and solute terms of the Köhler equation. The critical supersaturation for activation increases as aerosol radius decreases from an increase in surface tension and lower solute amount. Rose et al. (2010) found that the critical aerosol radius for activation at $0.87\text{--}0.07\%$ SS was about $20\text{--}100\text{ nm}$, which covers a smaller aerosol size range than the aerosol optical measurements. Small particles tend to have a higher organic fraction that often dominates the composition of fine mode aerosol. Compared to an equivalent mass fraction of inorganic salt, the lower water activity of organics may result in a slightly higher particle critical super saturation (Koehler et al., 2006). The effect of a potentially high organic fraction on fine mode aerosol activation is mixed. Ervens et al. (2005) found reduced droplet number concentrations over a wide range of updraft velocities in their cloud parcel model, but only for organic species with a solubility less than 20 g/L^{-1} , much lower than most or-

ganic acids found in ambient aerosol. However this study did not account for nonequilibrium conditions in clouds. Should the organic fraction form a soluble surfactant it could reduce the particle surface tension and lower the critical super saturation. Alternatively the organic fraction could form a hydrophobic layer that suppresses the uptake of water and raises the critical super saturation as was found by Kaku et al. (2006) in their study of marine aerosol. At SGP the gRH hygroscopic growth factors tend to decrease with particle size and indicate a high organic composition for particles less than $0.3\ \mu\text{m}$ diameter. These low growth factors in the subsaturated regime translate to critical super saturations in the range of 0.2 to 1.0 for sub $0.1\ \mu\text{m}$ diameter particles (Gasparini, 2006a, b), which is within % SS range of the CCN instrument. The comparison of CCN to aerosol optical properties assumes that the fine mode aerosol is essentially non-activating. The magnitude of this effect will increase at higher % SS and depend on the solubility of the organic compounds.

4 Results and discussion

The sites in this study are regional settings and as such represent aged aerosol of mixed composition. No one site has a characteristic single composition type to clearly distinguish it from the others. Instead the differences are subtle. Table 1 compares the average optical properties of the data used in the analysis between the four sites. The optical properties in Table 1 are only for sub μm particles at 450 nm and so ignore the coarse mode fraction. GRW and HFE have the smallest BSF and hence largest particles due to the influence of sea salt at GRW and probable dust at HFE. The likelihood of dust at HFE is supported from observation of construction in the region, the presence of a local cement factory and coal mine as well as low Ångström exponents and moderate to low hygroscopic growth factors typical of dust aerosol. The average SSA at GRW is unexpectedly low at 0.88 , which points to the influence of long-range transport of pollution aerosol as well as possible local pollution at the site despite extensive editing of short-duration data spikes to filter for local pollution. The data at GRW is biased toward times with higher aerosol loading, as the uncertainty of intensive properties at very low scattering and absorption signals was too high to include in the analysis. Both the HFE and FKB sites were influenced by frequent precipitation. The SSA was usually lower after a rain event as much of the highly soluble aerosol with higher SSA values may have been scavenged.

Initial analysis involved simple correlations of the aerosol extinction to the measured CCN. Figure 2 shows these correlations for submicron aerosol extinction at 450 nm . While a linear fit seems to characterize the Oklahoma data fairly well, the other three sites exhibit nonlinear behavior or multiple modes to the correlation that point to a more complex

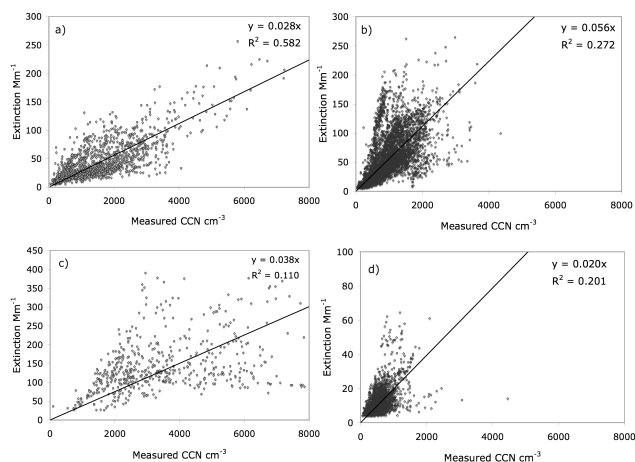


Fig. 2. Plots of aerosol extinction at 450 nm versus the measured CCN concentration at 0.4% SS from (a) Oklahoma (b) Black Forest (c) Hefei and (d) Graciosa.

behavior. No strong trend in the slopes with aerosol type is evident.

Figures 3 and 4 show the correlations between the power law fit parameters and the sub μm aerosol backscatter fraction and single scattering albedo. The fits from SGP use data that span 0.2 to 0.8% SS in steps of 0.20, 0.41 0.60 and 0.80 ± 0.01 . Ranges of % SS for the other sites are given in Table 1. Because of conditions of high aerosol loading at HFE the lowest % SS value at ~ 0.2 was not used in the analysis. The CCN instrument may have insufficient water or too short of a sample residence time for the aerosol to activate under high aerosol concentrations and low % SS (DMT, 2009).

In order to show a direct correlation to the backscatter fraction and hence aerosol size, the power law parameter C is normalized to the aerosol scattering coefficient at 450 nm. This normalized parameter, $C/\sigma_{\text{sp}}(450 \text{ nm})$, is the inverse aerosol scattering efficiency ($1/Q_{\text{sp}}$) in the case when 100% of the CN in the effective scattering size range activate. Figure 3 shows $C/\sigma_{\text{sp}}(450 \text{ nm})$ increases as the aerosol size decreases at higher backscatter fractions. At these sites the aerosol scattering increases faster with aerosol size than CCN formation. This slope varies with measurement site and likely reflects differences in the size-dependent aerosol composition at each site. The slope in Fig. 3 for GRW is significantly lower than the other three sites, which may reflect the aerosol sea salt composition as sea salt has a high scattering efficiency. The range of BSF at GRW was extended to 0.04 to accommodate the larger aerosol at this site and provide enough data for the fit calculation.

The k parameter indicates the steepness of the change in CCN concentration with % SS. Low values of k are typical of highly soluble aerosol such as sea salt and high k values of low-solubility aerosols. The range of k values (Table 2)

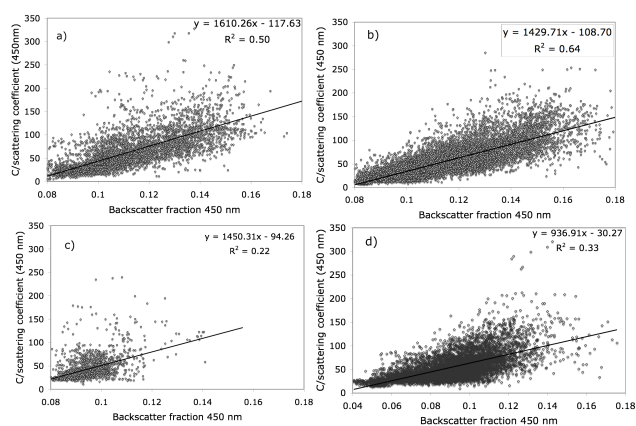


Fig. 3. Graphs of C /scattering coefficient (Mm cm^{-3}) versus backscatter fraction at 450 nm for (a) Oklahoma (b) Black Forest (c) Hefei and (d) Graciosa (note x-axis scale for graph d has a lower range).

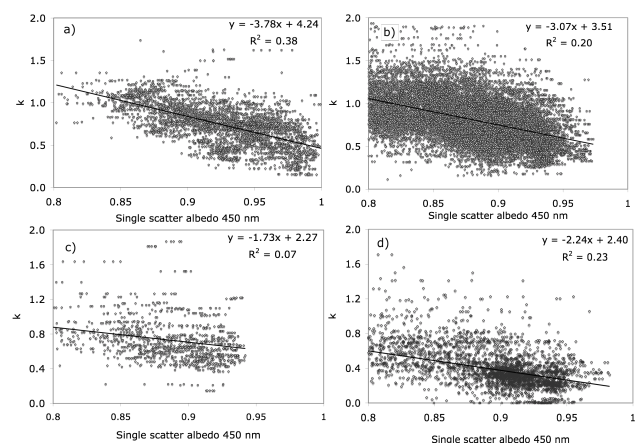


Fig. 4. Graphs of k parameter versus single scatter albedo at 450 nm for (a) Oklahoma (b) Black Forest (c) Hefei and (d) Graciosa.

and slope of k vs. SSA varies between sites. GRW has the lowest k values of 0.49 ± 0.43 and FKB has the highest k values with 1.06 ± 0.65 . The range of SSA at HFE doesn't extend higher than 0.941. At this site absorbing aerosol is ubiquitous and may reflect a high organic fraction. The slope of k vs. SSA at both HFE and GRW is low. For these sites changes in the aerosol absorbing fraction or equivalent black carbon (EBC) have a weak influence on CCN formation. In these instances other compounds may moderate CCN activation. At GRW the aerosol composition may have a high enough sea salt fraction to weaken the influence of organics on CCN. At HFE dust may moderate the influence of EBC on CCN. The higher slopes of k vs. SSA at SGP and FKB alternatively indicate a strong influence of EBC and other organics on CCN formation.

Table 2. Power law k fit parameter (± 1 std dev.), slope of power law fit versus measured CCN, and r^2 correlation coefficient of the fit to measured CCN.

Site	k	Slope	r^2
Oklahoma	0.73 (0.26)	0.94	0.89
Black Forest	1.06 (0.65)	0.95	0.96
Hefei	0.76 (0.33)	1.00	0.95
Graciosa	0.43 (0.42)	0.98	0.97

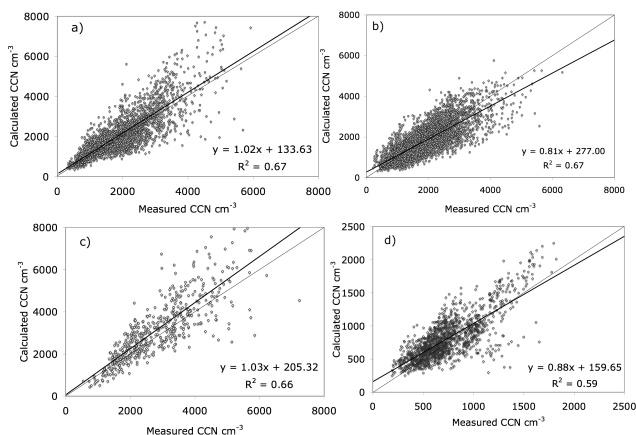


Fig. 5. Correlations of calculated versus measured CCN for (a) Oklahoma, (b) Black Forest, (c) Hefei and (d) Graciosa. Least square fit and 1:1 lines shown on each graph.

Figure 5 shows the fit correlations to the measured CCN across the full range of % SS for each site. All four sites exhibit good fits with r^2 correlation values of 0.66 or higher and slopes between 0.81 and 1.03. The goodness of the fits depends on both the ability of the power law fit parameters to represent the measured CCN as well as the correlation between the power law fit parameters, C and k , and aerosol BSF and SSA. For all of the fits the power law parameters underestimate the measured CCN by 4 to 11%.

Figure 6 gives a clearer view of the reason for the low slopes and positive intercepts in the correlations. The empirical model over estimates CCN at low measured CCN values. This over estimate is highest for FKB and hence results in a lower slope in Fig. 5. At the lower aerosol number concentrations the uncertainty in the calculated SSA and BSF values are higher. Another contributing factor to this uncertainty is the nonlinearity of the correlation between the k fit parameter and SSA, particularly at low SSA values. Despite these limitations the empirical fit is able to estimate the measured CCN within $\pm 50\%$ at the higher concentrations using only the aerosol optical properties as proxies for aerosol composition and size.

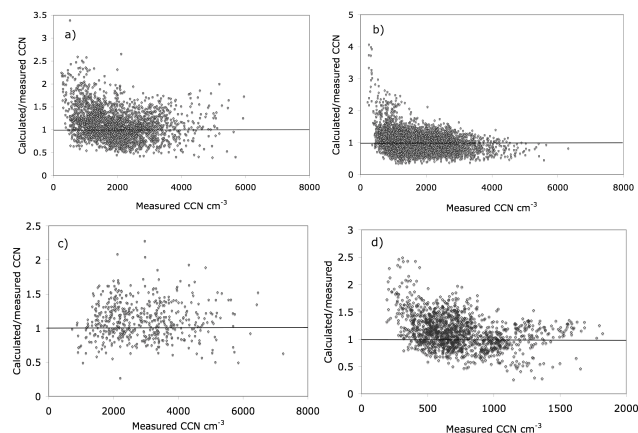


Fig. 6. Correlations of calculated/measured CCN versus measured CCN for (a) Oklahoma (b) Black Forest (c) Hefei and (d) Graciosa. Note the varying x- and y-axis scales for each graph.

5 Summary and conclusions

An empirical model uses the aerosol optical properties to estimate the measured CCN concentration as a function of percent supersaturation. The aerosol backscattering fraction and single scatter albedo act as proxies for the aerosol size and composition in the model. Relatively good agreement was found between the estimated and measured CCN values with higher uncertainties at low CCN concentrations.

The fit parameters varied with aerosol type and region. The slope of C/σ_{sp} (450 nm) vs. BSF was higher at continental sites and lower at a marine site. This parameter represents the inverse size-dependent scattering efficiency of the CCN and is therefore expected to be high for organic aerosol with low scattering efficiency and lower for sea salt, which has a high scattering efficiency.

The second fit parameter is the slope of k vs. SSA and signifies the relative growth of CCN with % SS as a function of the aerosol absorption or EBC content. For combustion aerosol the black carbon and total organic carbon content usually covary and the second parameter would be an indication of the effect of organic aerosol on CCN formation. This may not be the case for noncombustion organic aerosol. The slope of k vs. SSA varied between continental sites, a marine site and a site influenced by dust. At the marine site changes in the SSA had a weak influence on k and may indicate that a highly hygroscopic compound like sea salt can moderate the influence of less hygroscopic species like BC. Having even a small fraction of sea salt in the aerosol may be enough for the aerosol to activate even at low % SS, especially if the aerosol is relatively large as was the case at GRW. The slope of k vs. SSA was also low at HFE, which could be a factor of dust moderating the aerosol activation as well as high scatter and uncertainty in the data.

Considering that the optical measurements are insensitive to small particles that activate to CCN, the expectation for this method was to under estimate CCN. However no systematic under estimation was observed. Other factors in the method may compensate for this and warrants further study. In these particular cases the fine particle contribution may be small in comparison to the total CCN concentration.

This study is a first step in a process to better estimate CCN concentration as a function of % SS from the aerosol optical properties. Further analysis includes well-defined fit parameters for each aerosol type and region. This will entail analysis of the long-term data from SGP for seasonal trends of the fits and comparison to size-dependent aerosol composition to better quantify the fit parameters with aerosol type. Validation work is needed to test the method with vertically resolved in-situ aircraft measurements near clouds, surface measurements and remote sensing to see if the method can be extended further to include lidar or Cimel data.

Acknowledgements. I wish to acknowledge the ACRF support staff and technicians, especially Mike Alsop and Pat Dowell. I also thank Allison McComisky for helpful discussions.

Edited by: E. Weingartner

References

- Anderson, T. L., Covert, D. S., Marshall, S. F., Laucks, M. L., Charlson, R. J., Waggoner, A. P., Ogren, J. A., Caldow, R., Holm, R. L., Quant, F. R., Sem, G. J., Wiedensohler, A., Ahlquist, N. A., and Bates, T. S.: Performance characteristics of a high-sensitivity, three-wavelength, total scatter/backscatter nephelometer, *J. Atmos. Ocean. Tech.*, 13, 967–986, 1996.
- Anderson, T. L. and Ogren, J. A.: Determining aerosol radiative properties using the TSI 3563 integrating nephelometer, *Aerosol Sci. Technol.*, 29, 57–69, 1998.
- Andreae, M. O.: Correlation between cloud condensation nuclei concentration and aerosol optical thickness in remote and polluted regions, *Atmos. Chem. Phys.*, 9, 543–556, doi:10.5194/acp-9-543-2009, 2009.
- Bond, T. C., Anderson, T. L., and Campbell, D.: Calibration and intercomparison of filter-based measurements of visible light absorption by aerosols, *Aerosol Sci. Technol.*, 30, 582–600, 1999.
- DMT: Cloud Condensation Nuclei Counter Operator Manual, DOC-0086 Rev G-1, Droplet Measurement Technologies, Inc., p. 107, 2009.
- Ervens, B., Feingold, G., and Kreidenweis, S. M.: The influence of water-soluble organic carbon on cloud drop number concentration, *J. Geophys. Res.*, 110, D18211, doi:10.1029/2004JD005634, 2005.
- Ervens, B., Cubison, M. J., Andrews, E., Feingold, G., Ogren, J. A., Jimenez, J. L., DeCarlo, P., and Nenes, A.: Prediction of cloud condensation nucleus number concentration using measurements of aerosol size distributions and composition and light scattering enhancement due to humidity, *J. Geophys. Res.*, 112, D10S32, doi:10.1029/2006JD007426, 2007.
- Ervens, B., Cubison, M. J., Andrews, E., Feingold, G., Ogren, J. A., Jimenez, J. L., Quinn, P. K., Bates, T. S., Wang, J., Zhang, Q., Coe, H., Flynn, M., and Allan, J. D.: CCN predictions using simplified assumptions of organic aerosol composition and mixing state: a synthesis from six different locations, *Atmos. Chem. Phys.*, 10, 4795–4807, doi:10.5194/acp-10-4795-2010, 2010.
- Gasparini, R., Li, R., Collins, D. R., Ferrare, R. A., and Brackett, V. G.: Application of aerosol hygroscopicity measured at the Atmospheric Radiation Measurement Program's Southern Great Plains site to examine composition and evolution, *J. Geophys. Res.*, 111, D05S12, doi:10.1029/2004JD005448, 2006a.
- Gasparini, R., Collins, D. R., Andrews, E., Sheridan, P. J., Ogren, J. A., and Hudson, J. G.: Coupling aerosol size distributions and size-resolved hygroscopicity to predict humidity-dependent optical properties and CCN spectra, *J. Geophys. Res.*, 111, D05S13, doi:10.1029/2005JD006092, 2006b.
- Ghan, S. J. and Collins, D. R.: Use of In Situ Data to Test a Raman Lidar-Based Cloud Condensation Nuclei Remote Sensing Method, *J. Atmos. Ocean. Tech.*, 21(2), 387–394, 2004.
- Ghan, S. J., Rissman, T. A., Elleman, R., Ferrare, R. A., Turner, D., Flynn, C., Wang, J., Ogren, J., Hudson, J., Jonsson, H. H., VanReken, T., Flagan, R. C., and Seinfeld, J. H.: Use of in situ cloud condensation nuclei, extinction, and aerosol size distribution measurements to test a method for retrieving cloud condensation nuclei profiles from surface measurements, *J. Geophys. Res.*, 111, D05S10, doi:10.1029/2004JD005752, 2006.
- Good, N., Topping, D. O., Allan, J. D., Flynn, M., Fuentes, E., Irwin, M., Williams, P. I., Coe, H., and McFiggans, G.: Consistency between parameterisations of aerosol hygroscopicity and CCN activity during the RHaMBLe discovery cruise, *Atmos. Chem. Phys.*, 10, 3189–3203, doi:10.5194/acp-10-3189-2010, 2010.
- Heintzenberg, J., Wiedensohler, A., Tuch, T. M., Covert, D. S., Sheridan, P., Ogren, J. A., Gras, J., Nessler, R., Kleefeld, C., Kalivitis, N., Aaltonen, V., Wilhelm, R.-T., and Havlicek, M.: Intercomparisons and Aerosol Calibrations of 12 Commercial Integrating Nephelometers of Three Manufacturers, *J. Atmos. Ocean. Tech.*, 23(7), 902–914, 2006.
- Kaku, K. C., Hegg, D. A., Covert, D. S., Santarpia, J. L., Jonsson, H., Buzorius, G., and Collins, D. R.: Organics in the Northeastern Pacific and their impacts on aerosol hygroscopicity in the subsaturated and supersaturated regimes, *Atmos. Chem. Phys.*, 6, 4101–4115, doi:10.5194/acp-6-4101-2006, 2006.
- Koehler, K. A., Kreidenweis, S. M., DeMott, P. J., Prenni, A. J., Carrico, C. M., Ervens, B., and Feingold, G.: Water activity and activation diameters from hygroscopicity data – Part II: Application to organic species, *Atmos. Chem. Phys.*, 6, 795–809, doi:10.5194/acp-6-795-2006, 2006.
- Lance, S., Medina, J., Smith, J. N., and Nenes, A.: Mapping the operation of the DMT continuous flow CCN counter, *Aerosol Sci. Technol.*, 40(4), 242–254, 2006.
- McFiggans, G., Alfarra, M. R., Allan, J. D., Bower, K. N., Coe, H., Cubison, M., Topping, D. O., Williams, P. I., Decesari, S., Facchini, M. C., and Fuzzi, S.: Simplification of the representation of the organic component of atmospheric particulates, *Faraday Discuss.*, 130, 1–22, doi:10.1039/b419435g, 2005.
- McFiggans, G., Artaxo, P., Baltensperger, U., Coe, H., Facchini, M. C., Feingold, G., Fuzzi, S., Gysel, M., Laaksonen, A., Lohmann, U., Mentel, T. F., Murphy, D. M., O'Dowd, C. D., Snider, J. R., and Weingartner, E.: The effect of physical and chemical aerosol properties on warm cloud droplet activation, *At-*

- mos. Chem. Phys., 6, 2593–2649, doi:10.5194/acp-6-2593-2006, 2006.
- Petters, M. D. and Kreidenweis, S. M.: A single parameter representation of hygroscopic growth and cloud condensation nucleus activity, *Atmos. Chem. Phys.*, 7, 1961–1971, doi:10.5194/acp-7-1961-2007, 2007.
- Petters, M. D., Wex, H., Carrico, C. M., Hallbauer, E., Massling, A., McMeeking, G. R., Poulain, L., Wu, Z., Kreidenweis, S. M., and Stratmann, F.: Towards closing the gap between hygroscopic growth and activation for secondary organic aerosol – Part 2: Theoretical approaches, *Atmos. Chem. Phys.*, 9, 3999–4009, doi:10.5194/acp-9-3999-2009, 2009.
- Roberts, G. and Nenes, A.: A continuous-flow streamwise thermal-gradient CCN chamber for atmospheric measurements, *Aerosol Sci. Technol.*, 39(3), 206–221, 2005.
- Rose, D., Gunthe, S. S., Mikhailov, E., Frank, G. P., Dusek, U., Andreae, M. O., and Pöschl, U.: Calibration and measurement uncertainties of a continuous-flow cloud condensation nuclei counter (DMT-CCNC): CCN activation of ammonium sulfate and sodium chloride aerosol particles in theory and experiment, *Atmos. Chem. Phys.*, 8, 1153–1179, doi:10.5194/acp-8-1153-2008, 2008.
- Rose, D., Nowak, A., Achtert, P., Wiedensohler, A., Hu, M., Shao, M., Zhang, Y., Andreae, M. O., and Pöschl, U.: Cloud condensation nuclei in polluted air and biomass burning smoke near the mega-city Guangzhou, China – Part 1: Size-resolved measurements and implications for the modeling of aerosol particle hygroscopicity and CCN activity, *Atmos. Chem. Phys.*, 10, 3365–3383, doi:10.5194/acp-10-3365-2010, 2010.
- Sheridan, P. J., Delene, D. J., and Ogren, J.A.: Four years of continuous surface aerosol measurements from the Department of Energy’s Atmospheric Radiation Measurement Program Southern Great Plains Cloud and Radiation Testbed site, *J. Geophys. Res.*, 106(D18), doi:10.1029/2001JD000785, 2001.
- Sheridan, P. J., Arnott, W. P., Ogren, J. A., Andrews, E., Atkinson, D. B., Covert, D., Moosmüller, H., Petzold, A., Schmid, B., Strawa, A. W., Varma, R., and Virkkula, A.: The Reno Aerosol Optics Study: An Evaluation of Aerosol Absorption Measurement Methods, *Aerosol Sci. Technol.*, 39, 1–16, 2005.
- Shinozuka, Y., Clarke, A. D., DeCarlo, P. F., Jimenez, J. L., Dunlea, E. J., Roberts, G. C., Tomlinson, J. M., Collins, D. R., Howell, S. G., Kapustin, V. N., McNaughton, C. S., and Zhou, J.: Aerosol optical properties relevant to regional remote sensing of CCN activity and links to their organic mass fraction: airborne observations over Central Mexico and the US West Coast during MILAGRO/INTEX-B, *Atmos. Chem. Phys.*, 9, 6727–6742, doi:10.5194/acp-9-6727-2009, 2009.
- Solomon, S., Qin, D., Manning, M., Alley, R. B., Berntsen, T., Bindoff, N. L., Chen, Z., Chidthaisong, A., Gregory, J. M., Hegerl, G. C., Heimann, M., Hewitson, B., Hoskins, B. J., Joos, F., Jouzel, J., Kattsov, V., Lohmann, U., Matsuno, T., Molina, M., Nicholls, N., Overpeck, J., Raga, G., Ramaswamy, V., Ren, J., Rusticucci, M., Somerville, R., Stocker, T. F., Whetton, P., Wood, R. A., and Wratt, D.: Technical Summary, in: *Climate Change 2007: The Physical Science Basis, Contribution of Working Group I to the Fourth Assessment Report of the Intergovernmental Panel on Climate Change*, edited by: Solomon, S., Qin, D., Manning, M., Chen, Z., Marquis, M., Averyt, K. B., Tignor, M., and Miller, H. L., Cambridge University Press, Cambridge, United Kingdom and New York, NY, USA, 2007.
- Svenningsson, B., Rissler, J., Swietlicki, E., Mircea, M., Bilde, M., Facchini, M. C., Decesari, S., Fuzzi, S., Zhou, J., Mønster, J., and Rosenørn, T.: Hygroscopic growth and critical supersaturations for mixed aerosol particles of inorganic and organic compounds of atmospheric relevance, *Atmos. Chem. Phys.*, 6, 1937–1952, doi:10.5194/acp-6-1937-2006, 2006.
- Twomey, S.: The nuclei of natural cloud formation. II The supersaturation in natural clouds and the variation of cloud droplet concentration, *Pure Appl. Geophys.*, 43, 243–249, 1959.
- Virkkula, A., Ahlquist, N. C., Covert, D. S., Arnott, W. P., Sheridan, P. J., Quinn, P. K., and Coffman, D. J.: Modification, Calibration and a Field Test of an Instrument for Measuring Light Absorption by Particles, *Aerosol Sci.*, 39, 68–83, 2005b.